

**HERA-19 Commissioning: Closure Phases and Redundancy**  
**HERA Memorandum Number 15**  
**August 31, 2016**

C.L. Carilli<sup>1,2</sup>, J. Pober<sup>3</sup>, B. Nikolic<sup>2</sup>

ccarilli@aoc.nrao.edu

**ABSTRACT**

We analyze HERA19 data from March 11, 2016. We present uncalibrated visibility phases and amplitudes versus frequency for a number of redundant baselines. We then present closure phases versus frequency and time for a number of redundant triangles. The phase structure versus frequency for the raw visibilities show clear signatures of delay offsets (linear phase slope with frequency), but other effects of comparable magnitude. The shortest closure triangle shows a periodicity corresponding to the natural 'fringe rate with frequency' of the baseline. Comparing closure phase spectra for the shortest redundant triangles, we see similar behaviour overall, with a scatter between baselines over much of the frequency range of about  $15^\circ$  rms. We estimate this will cause dynamic range limitations in HERA-221 images of order  $10^3$ . Note that non-closing errors will not be fixed by standard antenna-based calibration. How these closure errors affect power spectra measurements remains to be determined. However, the smooth structure as a function of frequency suggests that frequency-domain estimates of the power spectra may be more robust to these errors.

**1. Introduction**

The closure phase is defined as the argument, or phase, of the product of three complex visibilities derived from three antennas (Thompson, Moran, & Swenson 2007). The equations

---

<sup>1</sup>National Radio Astronomy Observatory, P. O. Box 0, Socorro, NM 87801

<sup>2</sup>Cavendish laboratory, Cambridge University, UK

<sup>3</sup>Brown University, Providence, RI

are given in detail in HERA Memo 13, but to review, for measured visibilities for pairs of antennas in an interferometer,  $V_{i,j}^m$ , the triple product is defined as:

$$C_{i,j,k}^m = V_{i,j}^m V_{j,k}^m V_{k,i}^m$$

Assuming that all instrumentally induced complex gain terms can be factorized into a single amplitude and phase per antenna (eg.  $\theta_i$ ), then the phase of this complex triple product, or closure phase, is the sum of exponents:

$$\phi_{i,j,k}^m = \phi_{i,j}^s + (\theta_i - \theta_j) + \phi_{j,k}^s + (\theta_j - \theta_k) + \phi_{k,i}^s + (\theta_k - \theta_i) + \text{noise}$$

where  $\phi_{i,j}^s$  is the effective sky visibility. The antenna based phase calibration terms cancel in such a triangle, leading to:

$$\phi_{i,j,k}^m = \phi_{i,j,k}^s + \text{noise}$$

However, this conclusion relies on two assumptions. First is that the phase induced by the electronic system is factorizable into antenna based terms, ie. that the correlator or other aspects of the system do not introduce phase terms that depend on the particular cross correlation for a visibility.

And second, and more importantly for this memo, is the assumption that the effective sky visibilities measured by redundant baselines are identical. Non-redundancy can be due to two effects. First could be errors in antenna positions, ie. that the UV sample is not exactly the same for supposedly redundant spacings. For instance, at 2m wavelength, a 10cm position error for an antenna leads to a  $18^\circ$  phase error. Hence, accurate surveying of antenna locations is critical.

And second, the sky itself gets multiplied by the primary beam voltage pattern of each antenna. If these voltage patterns differ between antennas, then the product of voltage patterns will be different for each antenna pair, and hence the 'effective sky' (true sky  $\times$  product of antenna voltage patterns) will differ for each supposedly redundant baseline. If all the antennas were close to identical, then this should be a very minor effect, possibly arising only for the edge antennas of the array, due to cross coupling.

In the classic antenna-based calibration case for eg. the VLA or ALMA, the signal for the calibrators is completely dominated by emission in the very center of the field. Hence, any differences in primary beam shape, pointing, or sidelobe patterns is negligible, and the

standard assumptions about antenna-based gain separability are valid.<sup>1</sup>

For HERA, we have the much more complicated problem that the sky signal essentially fills the primary beam (main beam and sidelobes), including both diffuse Galactic emission and extragalactic point sources. Hence, any differences in the primary beam voltage patterns, including pointing errors, factor directly into real differences between measured visibilities for redundant baselines. In this case, the standard calibration assumption that the complex gains are factorizable into an amplitude and phase per antenna breaks down. This assumption is inherent to both sky-based calibration algorithms and redundant spacing calibration algorithms. In theory, the solution to this problem would be to measure the beams, then iterate through a 'self-calibration to sky model' loop that includes direction dependent gains for all antennas. In practice, such a process remains problematic.

Another way of looking at this is, assume our antenna efficiency (forward gain) is about 50% to 60%. By definition, this main beam efficiency implies that roughly half our power is coming from directions other than the main beam. If those directions are filled with emission with brightnesses comparable to the main beam, as is true at low frequencies, then any differences in the shape of the main beam and sidelobes leads to differences in the effective sky seen by the antenna.

The purpose of this memo is to investigate the closure phases for redundant antenna triangles in HERA, and thereby get a handle on the question: how redundant are our baselines? Closure analysis is also a powerful error diagnostic tool, providing a mean with which to investigate on the relative performance of antennas and baselines, independent of antenna-based calibration.

## 2. HERA-19 Data and Processing

The data are from the HERA-19 observations of March 11, 2016. We analyze a particular data set at LST 13:32, close to when Centaurus A is transiting. Cen A is at J2000 132527.61-430108.8, so about  $13\sigma$  off zenith<sup>2</sup>. The primary beam FWHM is about  $8^\circ$  and the declination for HERA zenith is -30:38. We also analyzed other time ranges and find similar results.

The data were processed to uvfits files using AIPY, including fringe-tracking on the

---

<sup>1</sup>In the old VLA broad band continuum correlator, closure errors arose due to differing bandpass shapes for the analog electronics for each antenna. This bandpass effect was directly analogous to what is being considered for the different primary beam power patterns herein.

<sup>2</sup>zen.2457458.53579.xx.HH.uvcUT.uvfits

mean zenith for the 10min data set. The data were then imported into CASA. CASA at NRAO has been updated with the HERA array in the Observatories table, and at this stage, CASA seems to be working with HERA data reasonably. The data were then averaged in time to 3min records, and exported via FITS to AIPS. AIPS can interpret the visibility data, but AIPS has a limit of 90 antennas. The antenna table has 127 antennas (a PAPER hold-over), so some AIPS tasks, like CALIB, do not work.

Figure 1 shows the array lay-out. We currently have three antenna numbering schemes. The red numbers are the CASA antenna ID numbers (I think also in AIPY). The yellow are the AIPS numbers (plus 1 wrt CASA). The numbers in the white boxes are the future HERA numbers, but these may change. Note that in CASA itself there are three nomenclatures: Antenna ID numbers (as above), Antenna Name, and Station Number. The Antenna Names are ID+1, like in AIPS. The stations numbers are the ID numbers. When IDs and Names are both numbers, CASA defaults to using the Names in tasks. For the analysis below, I use the AIPS numbers. In this case, antenna 82 is cross polarized.

The AIPS task 'UVPRT' was used to create ASCII tables of the visibility phases and amplitudes as a function of time or frequency. We then wrote python scripts to process these tables into closure phases and amplitudes, and for plotting and other processing. The important procedure here is to keep track of the signs of the phases (see equ. 2). UVPRT defaults to having the higher number antenna first. For closure phase calculation, the order of the antennas changes the sign, and hence a sign correction needs to be made in some cases.

The current processing is tedious, but forces us to look at the visibilities as a function of frequency and time in great detail. We are writing CASA tasks to generate closure quantities and both plot or write-out the values.

### 3. Results

#### 3.1. Visibility spectra

Figure 2 shows examples of uncalibrated visibility phases versus frequency over the full 100MHz to 200MHz band for a set of redundant (short, 14m) baselines for one 3min integration. In many cases, a significant, linear phase slope with frequency is apparent, corresponding to a standard (uncalibrated) delay offset. However, on top of these delays, there is significant structure with frequency. Some of this structure appears common between baselines, likely reflecting real structure of the redundant effective visibilities.

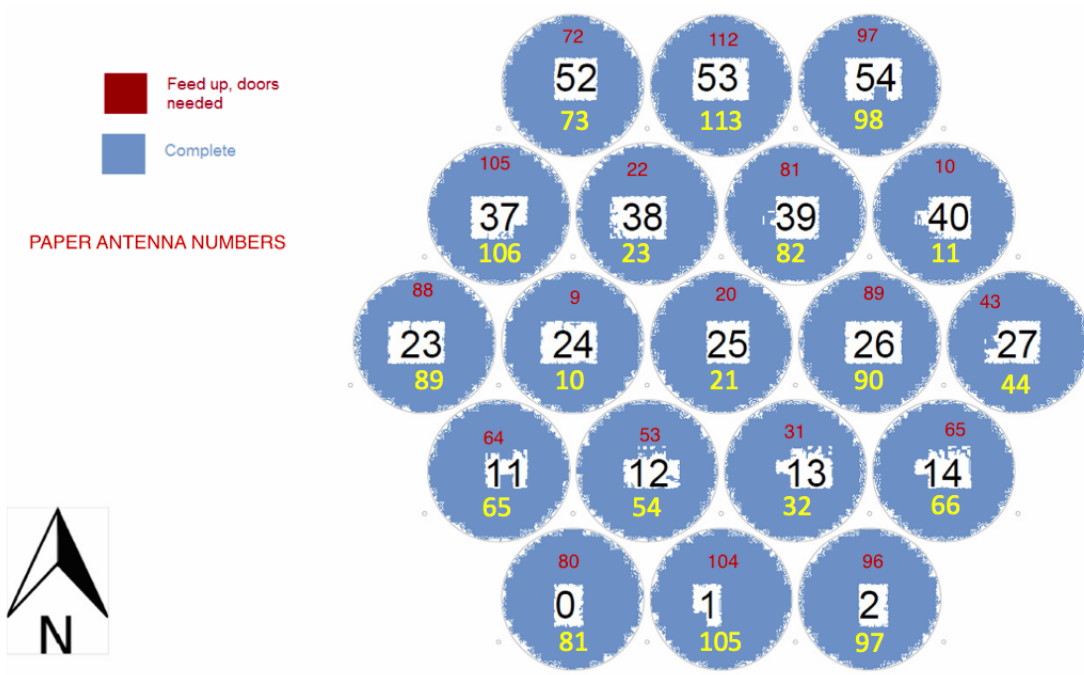


Fig. 1.— Positions and antenna numbers for HERA-19. The red numbers are the CASA antenna ID numbers. The yellow are the AIPS numbers (plus 1 wrt CASA). The numbers in the white boxes are the future HERA numbers, but these may change.

However, there are other differences that are not common, nor simply a linear phase slope with frequency. These could be antenna-based phase corrections due to electronics that might be calibrate-able using standard antenna-based phase-calibration methods. Or they could be differences due to closure errors (ie. non-redundancy of the effective baselines).

Note that, besides spectral index effects, the primary beam FWHM changes by a factor two from the lowest to the highest frequency, hence we expect significant changes to the visibilities over the full frequency range.

For completeness, Figure 2 also shows the uncalibrated visibility amplitudes versus frequency for the same set of redundant baselines. Again, there are similarities and differences that reflect the combination of true sky visibilities, antenna-based bandpass shape differences, and possibly non-closing errors.

### 3.2. Closure phase spectra

Figure 3 shows an example of the uncalibrated visibility phases, amplitudes, and closure phases, as a function of frequency. This example is for one equilateral triangles made up of the shortest baseline (14m). Note that in all cases herein, we adopt the antenna order convention in the closure phase calculation (i,j,k), starting with i at the apex (north) of the triangle, and j and k corresponding to a clockwise rotation around the triangle. While the visibility phases themselves show dramatic structure with frequency, as discussed above, the closure phases show a much more regular oscillating pattern.

This regular pattern with frequency corresponds to the natural ‘fringe rate with frequency’ for the short baselines  $\sim \cos(2\pi Bl/L)$ , where  $B$  is the baseline length,  $L$  is the wavelength, and  $l$  is the direction cosine ( $l \sim \cos(8^\circ) \sim 1$ ). For example, the middle of the band has  $L \sim 2\text{m}$ , and the wavelength of the peaks in the closure spectra occur at intervals  $\sim 0.33\text{m}$ . For a full cycle to occur over this interval, set  $\frac{2\pi B}{2.0} = X$ , and  $\frac{2\pi B}{2.0+0.33} = X - 2\pi$ . Differencing leads to:  $\frac{2\pi B}{2.0+0.33} - \frac{2\pi B}{2.0} = -2\pi$ , or  $B = 14\text{m}$ .

Figure 4 shows the closure phase versus frequency for all the shortest equilateral triangles in the array. They all show similar structure with frequency, indicating that, even without calibration, we are seeing direct evidence for the sky signal in the closure phases, as expected. However, technically these should be identical if the only differences were due to antenna-based calibration terms. The scatter then gives us a measure of the non-closing errors across redundant baselines. In other words, a standard antenna-based calibration process will not remove these differences in the closure spectra.

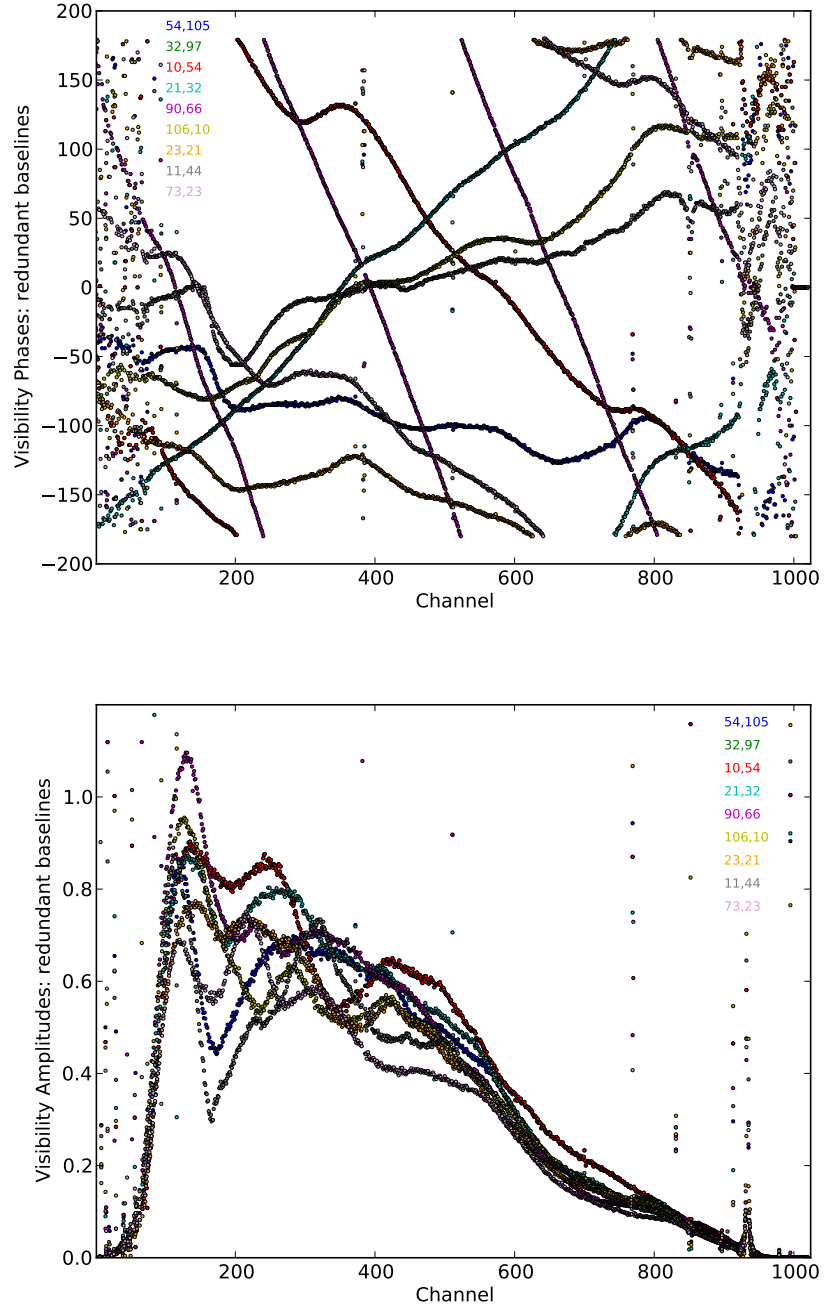


Fig. 2.— Uncalibrated visibility phases (top) and amplitudes (bottom) versus frequency for a 3min averaged record for HERA-19 data around 13:30 LST. These are all redundant 14m baselines.

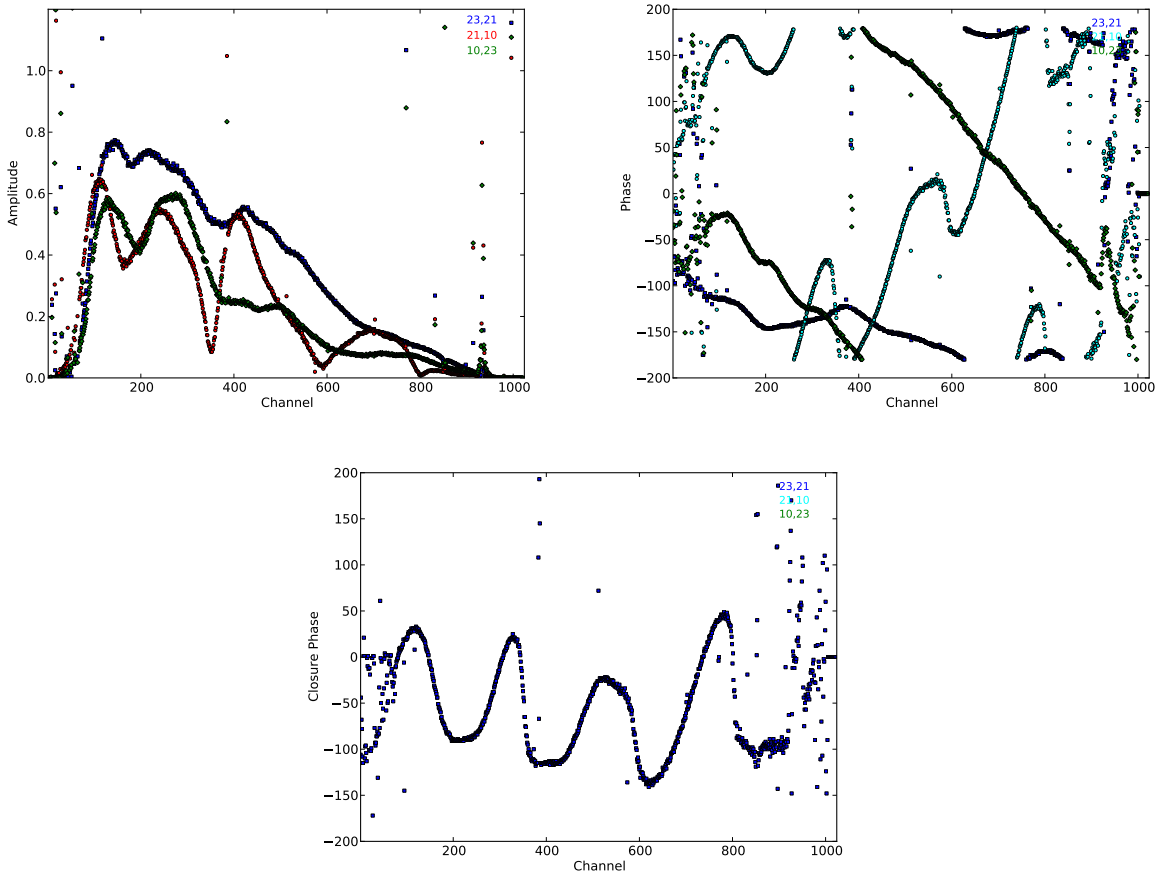


Fig. 3.— Uncalibrated visibility phases (top right), amplitudes (top left) and closure phase (bottom) for one short equilateral triangle versus frequency for a 3min averaged record for HERA-19 data around 13:30 LST.

Figure 5 shows the mean and rms deviation between antennas as a function of frequency for this set of short closure triangles. Over much of the spectrum, the rms deviations are  $\sim 15^\circ$ . We take this as a measure of our non-closing errors that would affect a standard antenna-based calibration technique. Since this rms entails 3 antennas, instead of 2, as would be the case for just the visibility phases, I think the value needs to be decreased by a factor  $\text{root}(2/3)$ , leading to rms phase errors:  $\phi_{rms} \sim 12^\circ = 0.21\text{rad}$  per baseline.

There are two other reasons that this rms may be higher than the true value. First, we are only using 9 input measurements, such that any outliers have an exaggeratedly adverse affect on the rms. And second, many of the triangles include duplicate antennas, meaning the 'noise' for some antennnas gets counted multiple times. Hence, the value above should be considered a conservative estimate of the non-closing errors of the current array, and these errors will fold directly into calibration errors using antenna-based calibration algorithms.

How will calibration errors of this magnitude affect imaging? The standard relation relating image dynamic range and calibration errors is given in Perley (1999):  $DNR \sim N/\phi_{rms}$ , where  $N$  is the number of antennas and  $\phi_{rms}$  is in radians. For HERA-221, the implied image dynamic range limit due to non-closing errors in antenna based calibration schemes is then:  $DNR \sim 10^3$ .

How will these errors affect power spectral measurements? That is not clear, but one might naively expect a similar order of magnitude (in Jy). However, there may be mitigating factors.

Figure 6 shows a blow-up of a 10MHz part of the closure spectra. On this scale, the closure phases for a given triangle are very smooth with frequency, and the dominant affect between baselines is just a slowly varying offset. Given that many of the current power spectral methods rely strictly on frequency dependent analysis, we can speculate that perhaps slowly varying offsets do not affect the final power spectrum as adversely? This remains to be tested, considering both closure amplitudes and phases, and through mock observations.

Figure 7 shows the closure phase for channel 400 over time for two redundant triangles. The record length is 10.7sec. The overall drift with time are similar, and slow.

We have only presented results for one 10min data set, and only for the shortest equilater closure triangle. However, we have analyzed other time ranges, and longer triangles, and the results are consistent with the  $15^\circ$  rms deviations presented in Fig 5.

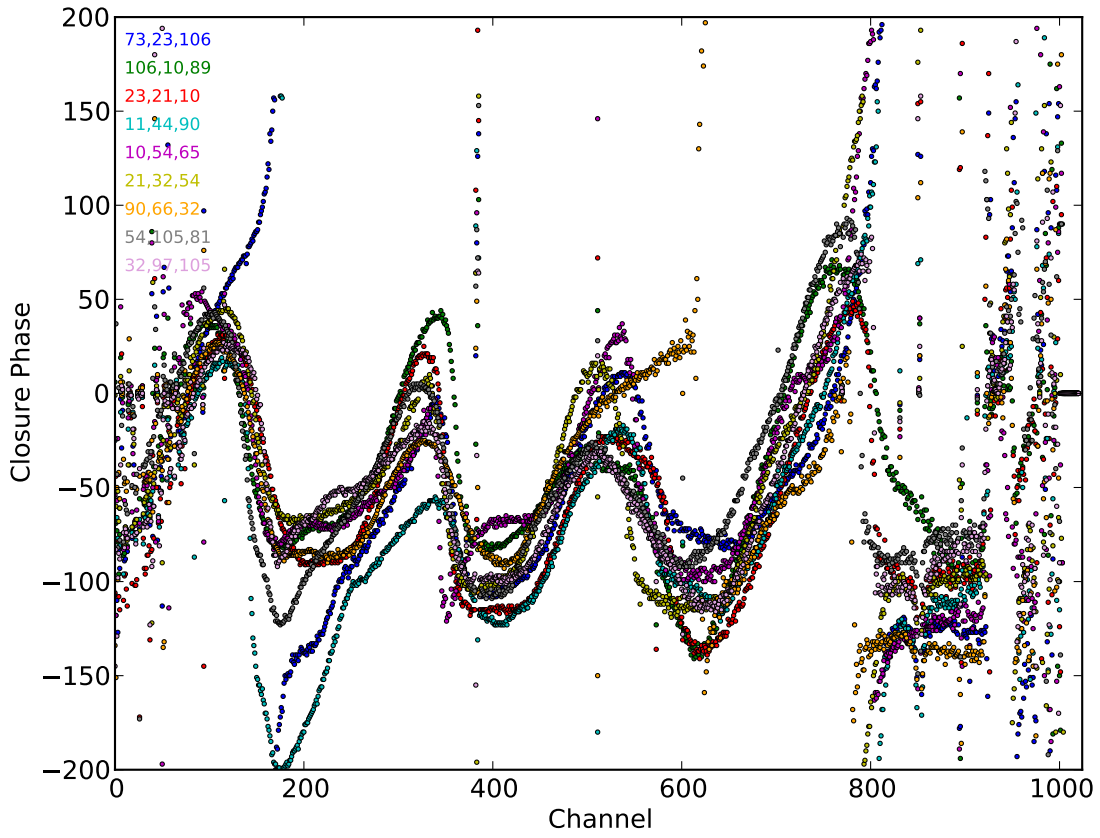


Fig. 4.— Closure phases versus frequency for all the shortest redundant equilateral triangles. Data is from a 3min averaged record for HERA-19 around 13:30 LST.

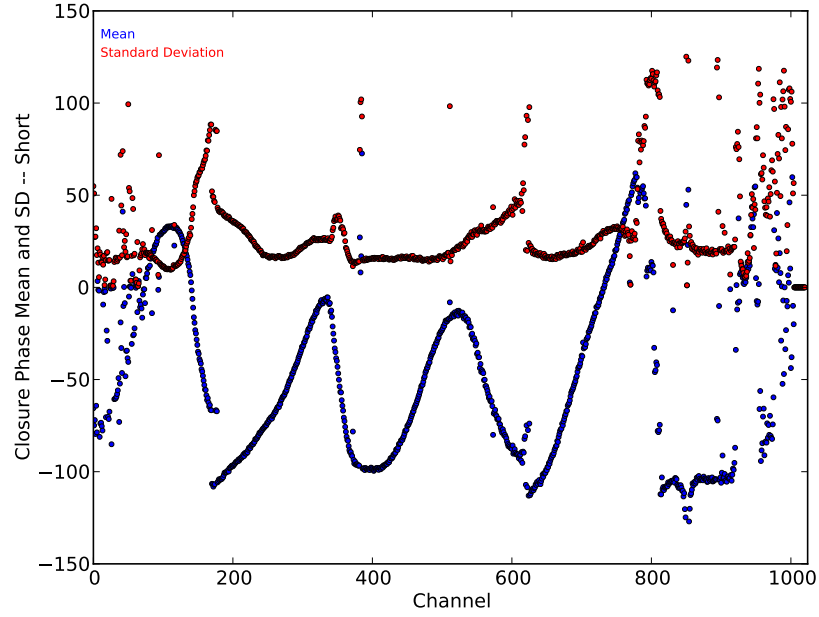


Fig. 5.— The mean and standard deviation between baselines at a given frequency for the Closure phases shown in figure 4.

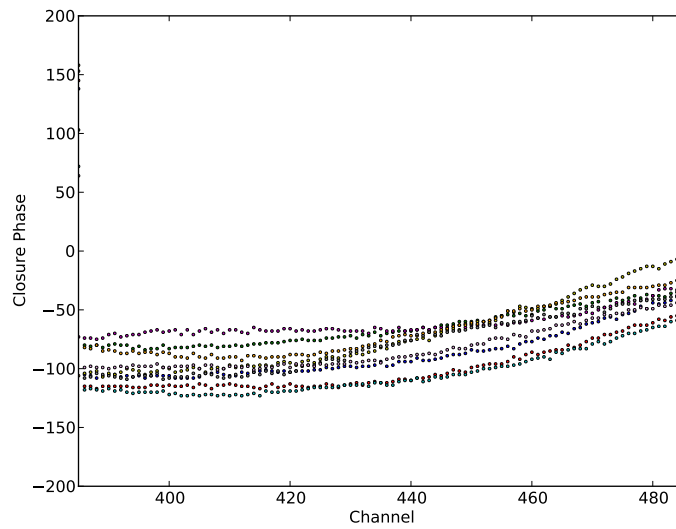


Fig. 6.— Same data as in Fig. 4, but now showing a blow-up of a 10MHz region of the spectrum.

## 4. Discussion

We find that the rms deviations of the closure phase measurements between 9 redundant triangles in HERA-19 data is about  $15^\circ$ . These errors fold directly into calibration errors using standard antenna-based calibration algorithms. We estimate errors of this magnitude will limit the imaging dynamic range of HERA-221 to about  $10^3$ . How calibration errors of this magnitude affect power spectral measurements remains to be determined.

The closure spectra are relatively smooth with time and frequency, and the differences between redundant triangles is typically just a slowly varying offset. This raises the speculation that power spectral measurement derived in the frequency domain might be more robust to the closure errors of the type seen herein.

How can non-closing errors be fixed? The obvious first step is to ensure accurate antenna positions, and as-identical-as-possible antenna primary beams, during construction. Precise construction will go a long way in ameliorating non-closing errors.

In terms of post-processing, standard antenna-based calibration (either using sky models or redundant calibration), will not fix these errors. One method that has been used in the quest for very high dynamic range imaging is baseline-based calibration, ie. to not assume that all calibration is separable into antenna-based terms. Unfortunately, this method is not necessarily over-constrained, and hence can easily 'turn the data into the model'. The standard method is to perform antenna-based calibration on short timescales, and then baseline-based calibration averaged over a very long timescale. The smooth behaviour in time and frequency of the closure phases for HERA-19 is encouraging from this perspective, but keep in mind that baseline-based calibration is a dangerous business.

The other solution is to do full direction dependent gain calibration, using whatever information is available for the primary beams, and building a wide-field sky model of both diffuse and point source emission in the process. This process has not been developed to date, and may even violate information theory in the extreme case being considered herein.

In future memos we will explore the CASA tools for generating closure quantities, and investigate closure amplitudes, and using closure quantities for error diagnostics and flagging.

## References

- Carilli, C. & Sims, P. 2016, HERA memo 13 (<http://reionization.org/science/memos/>)
- Perley, R. 1999, in *Synthesis Imaging in Radio Astronomy II*, eds. G. B. Taylor, C. L. Carilli, and R. A. Perley. ASP 180, 1999, p. 275

Thompson, A.R., Moran, J., Swenson, G. 2007, *Interferometry and Synthesis in Radio Astronomy*, John Wiley & Sons, 2007

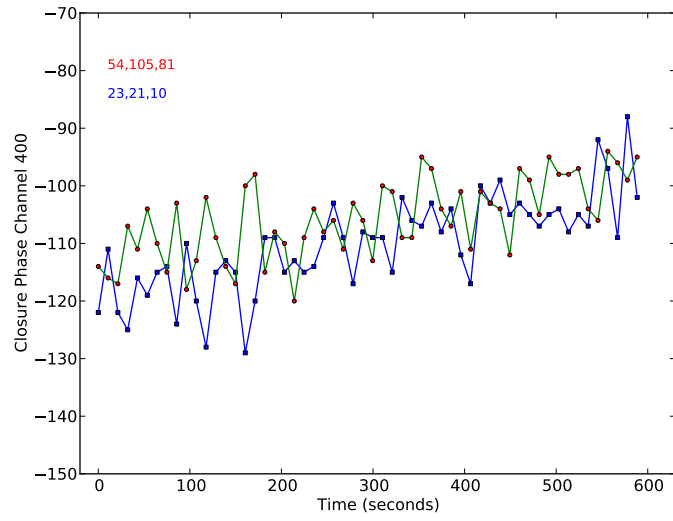


Fig. 7.— The Closure phases for channel 400 over 10.7min using 10second records for two redundant short triangles.